Available online at www.sciencedirect.com
ScienceDirect
Journal of the European Ceramic Society 27 (2007) 1961–1972
www.elsevier.com/locate/jeurceramsoc

In situ observation of the direct and indirect dissolution of MgO particles in $CaO–Al_2O_3–SiO_2$-based slags

J. Liu *, M. Guo, P.T. Jones, F. Verhaeghe, B. Blanpain, P. Wollants

Department of Metallurgy and Materials Engineering, Katholieke Universiteit Leuven, Kasteelpark Arenberg 44, BE-3001 Heverlee, Leuven, Belgium

Received 22 February 2006; received in revised form 15 May 2006; accepted 20 May 2006
Available online 1 August 2006

Abstract

The dissolution of magnesia particles in synthetic $CaO–Al_2O_3–SiO_2$ (CAS)-based slags with and without MgO addition was investigated *in situ* with a confocal scanning laser microscope (CSLM) at 1500 and 1600 °C. The dissolution process was recorded. The effects of slag composition and temperature on the dissolution process and the time dependency of the MgO particle size during dissolution were obtained. Increasing the temperature increases the dissolution rate. However, MgO addition to the slag retards the dissolution rate significantly. The rate limiting steps are discussed. It is shown that boundary layer diffusion is responsible for the dissolution. By combining *in situ* observations with post mortem analyses, thermodynamic calculations of local and global equilibrium, and kinetic considerations, the conditions under which $MgAl_2O_4$ spinel can be formed at the particle–slag interface are clarified.

Keywords: CSLM; Corrosion; MgO; Spinel; $CaO–Al_2O_3–SiO_2$ base slags

1. Introduction

Dissolution of solid oxides such as magnesia into slag melts can occur either through a direct or an indirect mechanism. In the case of indirect dissolution, the oxide dissolves into the melt by first forming an intermediate, solid reaction product at or near the oxide/melt interface.[1–3] The process of indirect dissolution may be rate limited by a chemical reaction, by solid-state diffusion through the reaction product, by liquid-phase diffusion through the boundary layer, or by a combination.[4] Typical examples of indirect MgO dissolution include the formation of a dense spinel ($MgO·Al_2O_3$) or magnesiowustite ((Mg,Fe)O)/((Mg,Fe,Mn)O) layer, which protects the MgO from further degradation.[5–8]

Understanding the nature of oxide dissolution into a slag phase is relevant for at least three applications. In the case of refractory materials, one may target slow, indirect dissolution in order to enhance the service lifetime of the refractory lining. In the other two cases one requires fast dissolution. When one deals with oxidic inclusions during (clean) steel production, inclusions need to dissolve promptly into the slag phase. If the kinetics of dissolution is not sufficiently fast, non-dissolved inclusions will rest near the interface and thereby increase the risk of re-entrainment.[9] Thirdly, when one deals with slag additives, such as dolomite and doloma in primary steelmaking processes (BOF and EAF processes), one normally expects a rapid dissolution. Doloma and dolomite are used in steel refining as fluxing additions as well as lime to obtain a basic slag for the removal of oxidation products and sulphur. They enhance the dissolution of lime into the molten slag by forming an early basic slag at the start of refining. As with inclusion oxides, dolomite and doloma need to dissolve rapidly into the slag phase. The mechanisms by which dolomite and doloma dissolve into a model BOF slag in the system $CaO–MgO–SiO_2–FeO–MnO$ were studied by Satyoko and Lee.[10]

The most common method used to investigate the dissolution mechanisms of solid oxides into liquid slags and their kinetics involves finger test techniques whereby a refractory material is dipped into a molten slag and exposed for a certain period. The dipped refractory sample may be positioned statically or may be rotated, as is the case in the classical rotating finger or disk method. After completion of the test, the finger is removed and analyzed (post mortem) for slag penetration and/or corrosion. The dip technique is a reliable and simple method that has been used for generating relevant data.[1,4,11] Especially with

* Corresponding author. Tel.: +32 16321213; fax: +32 16321991.
E-mail address: junhu.liu@mtm.kuleuven.be (J. Liu).

0955-2219/$ – see front matter © 2006 Elsevier Ltd. All rights reserved.
doi:10.1016/j.jeurceramsoc.2006.05.107

the rotating method, it is possible to extract the rate controlling mechanism of the dissolution process.

However, post mortem determination of dissolution mechanisms and kinetics suffers from being an elaborate and intrinsically indirect procedure. Recently, a new technique has become available which offers a complementary approach. The high-temperature confocal scanning laser microscope combined with an infrared image furnace (CSLM-IIF) allows for *in situ* observations of the dissolution behaviour of micro-particles in a slag. One requirement is that the slag needs to be transparent for laser light. This excludes slag systems that contain transition metal oxides such as FeO and CrO_x. However, for transparent slags, it is possible to complement the previously mentioned post mortem procedure with the *in situ* dissolution behaviour of micro-particles. CSLM work has been done on the dissolution kinetics of MgO, Al_2O_3 and/or $MgAl_2O_4$ micro-particles in $CaO–SiO_2–Al_2O_3$(–MgO),[9,12,13] $CaO–Al_2O_3–MgO$[14] and $SiO_2–Al_2O_3–MgO$[15] slag systems. The main attention has gone out to determine the rate controlling step of the dissolution process. Some of these studies[9,12,14] highlighted the possibility of indirect MgO dissolution (through the formation of a $MgAl_2O_4$ spinel layer). Nevertheless, for the $CaO–SiO_2–Al_2O_3$ system, the maximum temperature involved was 1530 °C,[9,12] which is substantially lower than actual steelmaking temperatures. Considering that the formation of spinel is highly sensitive to temperature and that the conditions under which it forms remain unclear, additional work is required to fully understand the dissolution of MgO particles in slags under steelmaking conditions.

In the present CSLM work, the focus is on the *in situ* direct observation of the dissolution of MgO particles at temperatures up to 1600 °C. The chosen slag system is $CaO–SiO_2–Al_2O_3$ based, with and without the initial presence of slag MgO. The choice for MgO as solid oxide is two-fold. Magnesia is the base material for a number of important refractory types (including magnesia–carbon, magnesia–chromite, and magnesia–spinel) that are used in steel processing vessels. Likewise, exogeneous MgO also occurs as a typical inclusion particle during the production of steel.[15] It is, therefore, of paramount importance to study the dissolution behaviour of MgO in typical slag systems. Special attention is given to the possibility of *in situ* formation of an intermediate spinel layer around the magnesia particle which would be beneficial for the sake of refractory protection but detrimental in the case of inclusion dissolution. Direct observations are coupled with post mortem analyses, kinetical considerations and thermodynamic calculations using the FactSage© and ChemApp© software packages. We make a distinction between global and local equilibrium, which clarifies the conditions under which indirect dissolution may occur. Through the combination of these techniques the nature of the dissolution mechanism of MgO particles in $CaO–SiO_2–Al_2O_3$(–MgO) slags is unravelled.

2. Experimental

A confocal scanning laser microscope with a high temperature cell (CSLM, Lasertec, 1LM21H-SVF17SP) was used. In the CSLM, high resolution (0.25 μm) images of a material can be obtained that cannot be produced by most other conventional imaging techniques. Such imaging enables real time *in situ* observation of high temperature (up to 1700 °C) transient phenomena. The CSLM allows observation at any plane between the surface of the transparent slag and the bottom of the crucible. The advantages of the CSLM technique with reference to traditional dissolution experiments of rods and cylinders are twofold. The CSLM method allows for continuous *in situ* observation as opposed to post mortem analysis of quenched samples. Furthermore, the ratio of volume of dissolving species to the volume of solvent slag is small. Therefore, dissolution takes place without significant changes in the bulk composition of the slag. Details of the CSLM technique have been published elsewhere.[16,17]

Table 1
Composition (mass%) of the slags used in this study as determined with EPMA-WDS

	CaO	Al_2O_3	SiO_2	MgO	Basicity (C/S)
Slag A	29.7	24.1	46.2	<0.5	0.65
Slag B	29.9	23.5	39.3	7.3	0.76

The composition of the slags used in this study as determined with EPMA-WDS is given in Table 1. CaO, MgO, Al_2O_3, and SiO_2 are slag components that aggressively attack refractory materials in industrially important processes.[18,19] The slags were prepared by mixing the oxide compounds and melting the mixture in a molybdenum crucible in a tube furnace under Ar (1600 °C, 24 h). After melting, the slag was quenched against a steel plate and crushed to powder. This powder was then melted in the CSLM to release all the gases absorbed by the powder prior to running an experiment.

The dissolution studies took place in a platinum crucible (5 mm in diameter and a height of 4.5–6 mm) by placing one MgO particle of 350–400 μm radius on the surface of a solid slag and heating this assembly to the desired temperature under an ultra-high purity Ar atmosphere. Fig. 1 shows the sample holder assembly. The added MgO particle constituted 0.09–1.3% of the total slag sample weight. The source of MgO particles was fused lump (1–3 mm, Alfa Aesar) with a purity of 99.95%.

The thermal cycle during the dissolution experiment is of great importance and should allow the slag to melt before initiating the dissolution process. Therefore, the sample was heated from an intermediate temperature of 1000 °C up to the desired

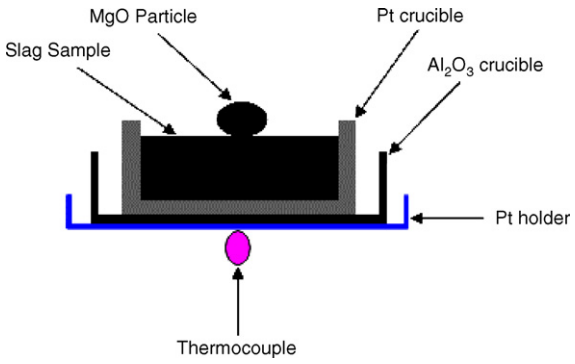

Fig. 1. Schematic representation of the CSLM specimen holder.

experimental temperature within 2–3 min. The sample temperature was measured by a B-type thermocouple welded on the bottom surface of the Pt holder. The temperature accuracy was confirmed by melting experiments of pure copper, pure nickel and pure iron. Experiments were conducted at 1500 and 1600 °C. Once the slag melted and the particle submerged, the size of the particle was monitored as a function of time through the transparent molten slag.

The video recordings of the dissolution process were analyzed to obtain the change in particle area with time. The procedure involved capturing and digitizing images from the video, then reading the digitized image into a public domain image analysis software.[20] Once in the digital analysis system, a border was manually drawn around the MgO particle. On the assumption that the particle is a sphere, a radius of an equivalent circle was computed at defined time intervals. It is this calculated equivalent radius that forms the basis of the results presented in this paper.

In order to study the slag/particle interface, after the experiment at 1600 °C in slag B the Pt crucible was cross sectioned with a diamond saw, and one half of the specimen with MgO particle was ground and polished. The polished specimen was coated with a conductive carbon layer to allow characterisation of the particle/slag interface by a scanning electron microscope (Philips XL30 FEG) equipped with an energy dispersive spectroscopy detector, and an ARL electron microprobe equipped with a wavelength dispersive spectroscopy detector (EPMA-WDS). Characterisation included documentation of the microstructure of the corrosion products using the backscattered electron imaging mode with Philips XL30 FEG and quantitative chemical analysis of the corrosion products with ARL electron microprobe.

3. Results and discussion

3.1. Behaviour of MgO particles during dissolution

3.1.1. Rounding of angular particles

The initial shape of the particle before the dissolution experiment was angular. After some time the surface of the dissolving particle became rounder. Fig. 2 shows this phenomenon. During refractory corrosion, solid phases dissolve. As a consequence the composition of adjacent liquid changes locally. The first components of the refractory material that dissolve tend to be those with the highest solubility. Smaller particles with small radius of curvature and angular shaped protruberances have higher specific surface areas and higher dissolution rates. Removal of the angular shaped protruberances of a dissolving particle leads to a rounding of the particle.[21]

3.1.2. Dissolution and detachment

The MgO particle used in this study is built up by small subgrains thus containing an intragranular network of grain boundaries. In the present corrosion study, detachment is defined as the removal of minor fragments from the dissolving MgO particle. On the other hand, dissolution is defined as the slow and gradual removal or diffusion of MgO from the dissolving particle into the slag. Both detachment and dissolution were observed in this study. Fig. 3 illustrates these phenomena at 1500 °C in slag A.

Refractories are generally made as prefired shapes (bricks) or as unfired monolithic materials installed by, for example, casting or gunning before *in situ* drying and firing. The resulting microstructure typically consists of large (up to several mm) aggregates, grains or filler held together by a finer, more porous bond or matrix. The higher porosity and fine texture of the bond make it more reactive than the grain. This leads to the preferential corrosion of the bond and detachment of big particles from the main refractory body.

3.1.3. Particle rotation

During dissolution the dissolving particle rotates. Fig. 4a shows the dissolution curve of a MgO particle. A rotation period of 38–46 s is observed (Fig. 4b). The oscillation of the equivalent radius of the MgO particle during dissolution is probably due to the non-spherical character of the particle. During the dissolution process, the build-up of a composition profile near the particle surface could be responsible for changes in slag properties and associated mass fluxes. If the particle is not spherical, there could be a change in the local radius that will result in locally varying mass fluxes that could produce rotation. Because of rotation, the measured average radius decreases in an oscillating way. Rotation of the particles introduces errors and hinders the determination of the dissolution mechanism. Rotation can also affect the rate limiting mechanism since this motion may alter the diffusion fields around the particle.

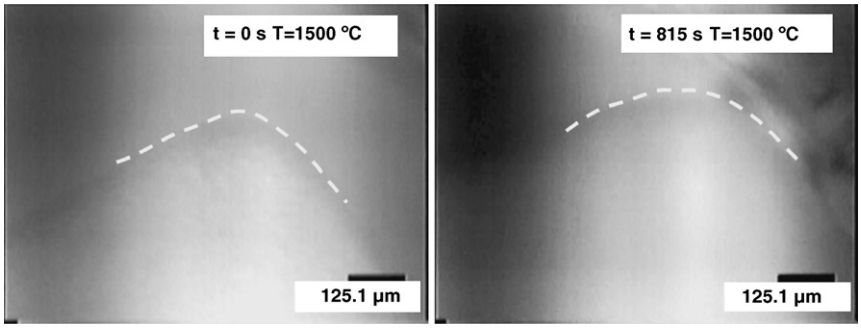

Fig. 2. Dissolution leads to rounding of angular particles.

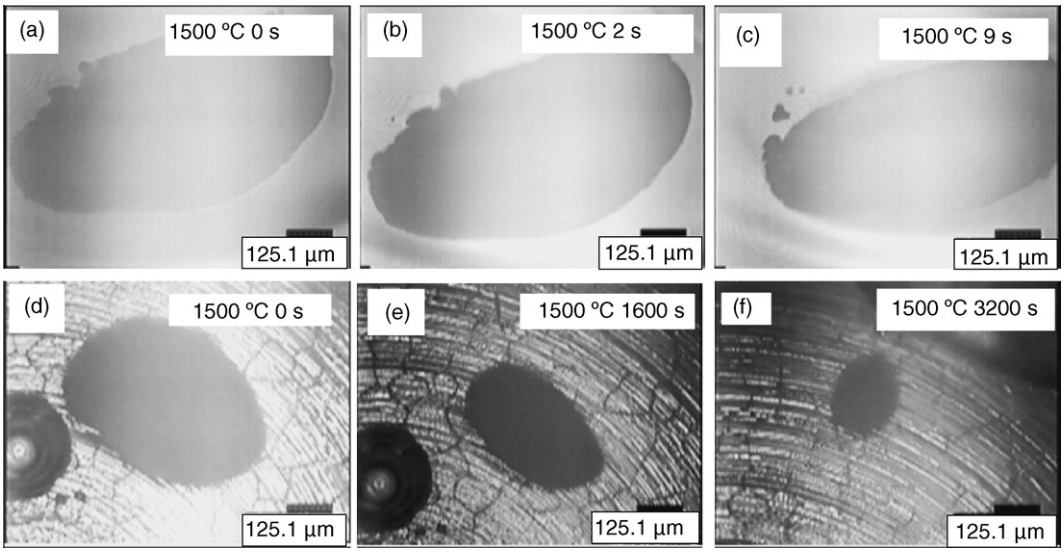

Fig. 3. Detachment (a–c) and dissolution (d–f) in slag A.

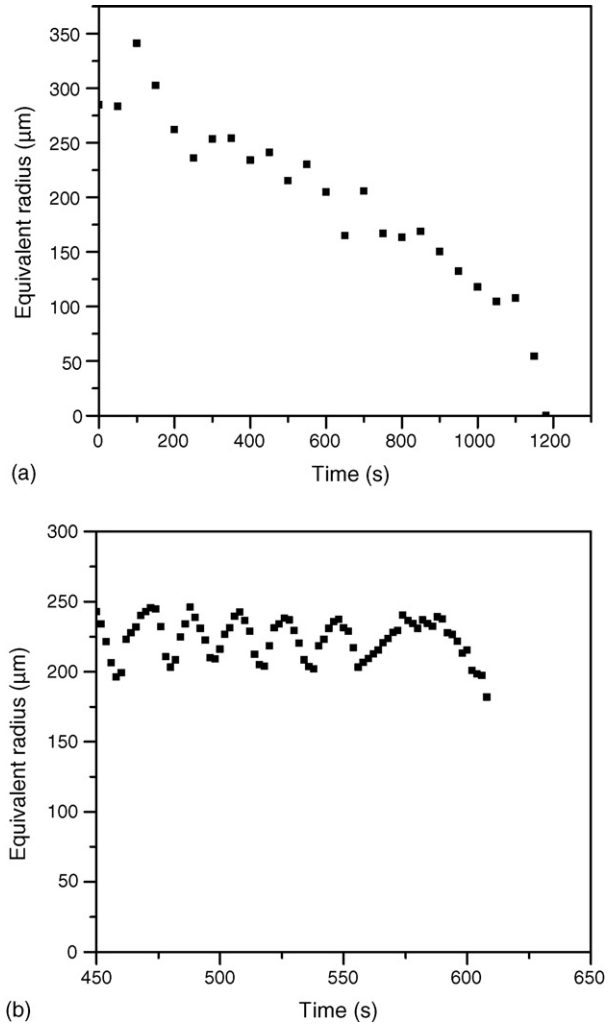

Fig. 4. (a) Dissolution curve of a rotating MgO particle in slag A at 1500 °C. (b) Detail of dissolution curve in (a) of one rotating MgO particle.

The shape of the particle is an important source of scatter in the total dissolution time. The equivalent radius was calculated by assuming that the particle is spherical. Due to the particle rotation it could be observed that this is not always the case: some particles were flat (lenses) or slender (cylinders).

3.2. Dissolution mechanism

In order to investigate the dissolution mechanism of MgO, the classical shrinking core reaction models were used.[22] We considered as rate-determining steps: (1) surface reaction (Eq. (1)) and (2) boundary layer diffusion in the Stokes regime (Eq. (2)). In the case of surface reaction:

$$\frac{R}{R_0} = \left(1 - \frac{t}{\tau}\right) \tag{1a}$$

and

$$\tau = \frac{\rho R_0}{k(C^{(p)} - C^{(s)})} \tag{1b}$$

where R and R_0 are the actual and initial radius of the dissolving MgO particle, ρ its density, t and τ the actual and total dissolution times, k the reaction rate constant and $(C^{(p)} - C^{(s)})$ is the difference between the concentration of MgO in the slag (s) and the concentration of MgO in a saturated slag in equilibrium with the MgO particle (p). This concentration difference is the driving force for dissolving the MgO particle. In the case of boundary layer diffusion:

$$\frac{R}{R_0} = \left(1 - \frac{t}{\tau}\right)^{1/2} \tag{2a}$$

and

$$\tau = \frac{\rho R_0^2}{2D(C^{(p)} - C^{(s)})} \tag{2b}$$

where D is the diffusion coefficient of the slowest diffusing species resulting from the dissolution process, which needs to be transported into the bulk slag across the boundary layer.

If R/R_0 is plotted versus t/τ, the dissolution mechanism can be determined from the resulting curve. According to Eq. (1a), dR/dt is constant, and the dissolution curve is a straight line. However, according to Eq. (2a), dR/dt increases as the particle radius decreases. Fig. 5a shows the actual dissolution curves for the MgO particles.

From Fig. 5a it is difficult to verify the dissolution mechanism by direct comparison of the experimental results with the theoretical curves. However, if we look at the average dissolution curve (curve generated from the average data) of the experimental results shown in Fig. 5b, we may conclude that boundary layer diffusion controls the dissolution of MgO particles in this study, although the average dissolution curve does not fit the theoretical curve perfectly. Some reasons for the deviation are: the rotation of the dissolving particles and the definition of the particle boundary in the image analysis procedure.

3.3. Kinetic considerations of the dissolution process

3.3.1. Effect of temperature

Fig. 6 shows the equivalent radius, R, versus time, t, curves for MgO particles dissolving in slag A, respectively, at 1500 and 1600 °C. It is clear that the dissolution rate increases with increasing temperature. If we ignore the minor change in slag composition (MgO content) caused by the dissolution of MgO particles, we can see from Fig. 6 that starting from an equivalent radius of about 305 μm, the MgO particle dissolved in the slag in 83 min at 1500 °C and in 39 min at 1600 °C.

3.3.2. Influence of temperature and slag composition

The dissolution rate of an MgO particle is strongly influenced by the composition of the slag (Fig. 7). Initially, slag A contains no MgO and therefore the driving force for dissolution in slag A is high. Slag B initially contains 7.3% MgO (solubility limit ± 11.5%) and therefore the driving force for dissolution in slag B is lower.

If local equilibrium is assumed at the particle/slag interface, the driving force for MgO dissolution is related to the concentration difference of MgO between the particle/slag interface and the bulk of the slag. The former can be evaluated from the phase diagram, where it is given by the saturation limit. Both temperature and slag composition have marked effects on the dissolution rate of MgO through the change of this driving force. The effects of temperature and slag composition can be explained with reference to the $CaO–Al_2O_3–SiO_2–MgO$ phase diagram. Ignoring the presence of minor constituents, the compositions of slags A and B are shown in the $CaO–Al_2O_3$ (25 mass%)$–SiO_2–MgO$ phase diagram (Fig. 8). One can see that increasing the temperature from 1500 up to 1600 °C enhances the saturation limit of MgO in slag A from about 12.5–19 mass%. Thus, the con-

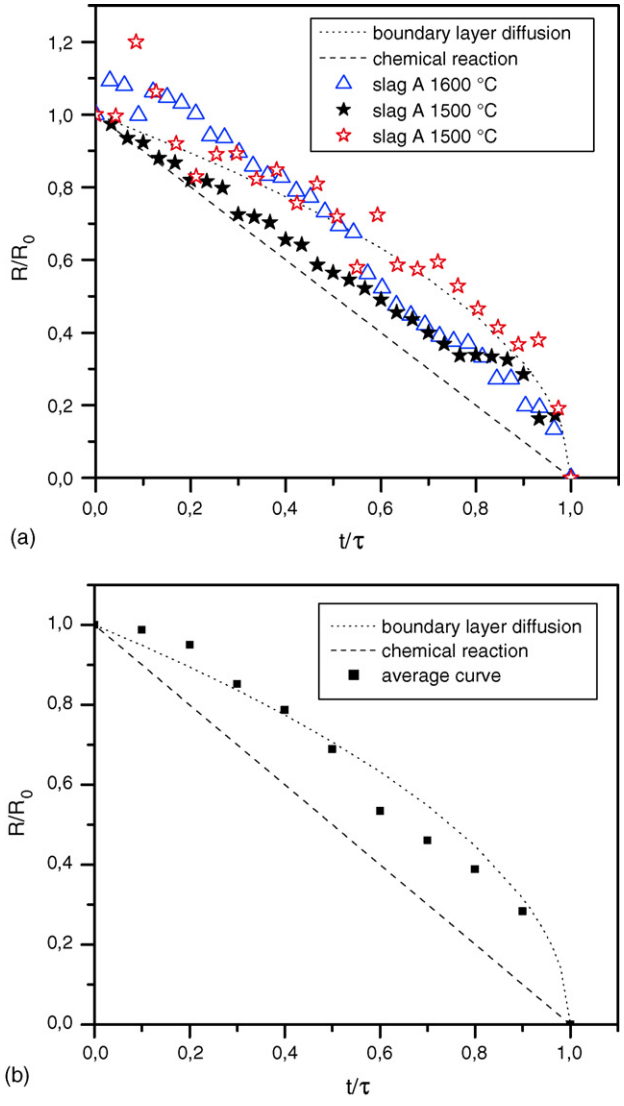

Fig. 5. (a) Normalised dissolution curves for MgO particles in CAS slags. (b) Average dissolution curve for MgO particles in a CAS slag.

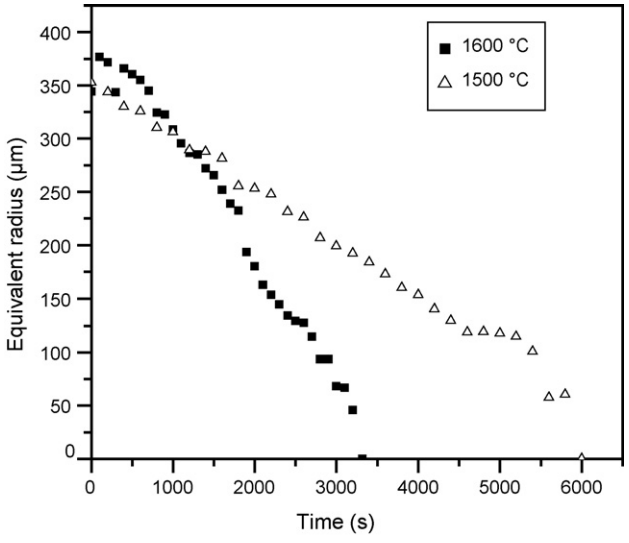

Fig. 6. Evolution of equivalent radius of fused MgO particles in slag A at different temperatures.

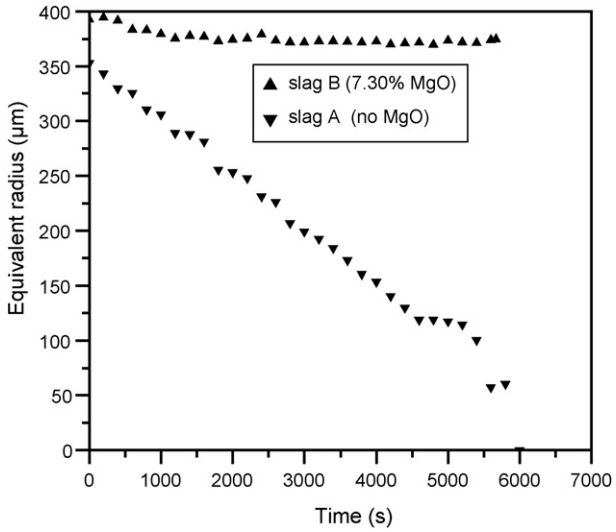

Fig. 7. Effect of slag composition on the dissolution rate of MgO particles at 1500 °C.

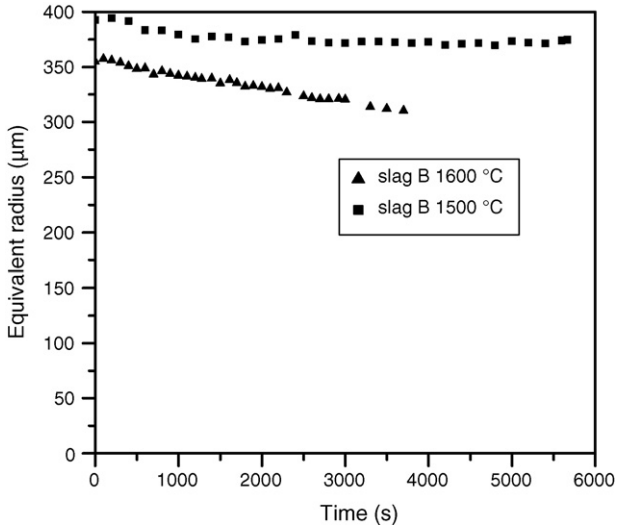

Fig. 9. Dissolution curves of MgO in slag B.

centration difference is enlarged, and the driving force for MgO dissolution is increased. Moreover, the increase in temperature accelerates the diffusion process. Therefore, higher temperatures lead to a faster dissolution rate and a decrease in dissolution time, as was observed. As expected, increasing the initial MgO content in the slag (slag A → slag B) decreases the amount of MgO that can be dissolved thermodynamically. This leads to a decrease in the driving force for MgO dissolution as expressed by the concentration difference between the slag/particle interface and the bulk of the slag (the difference being reduced in this case from 12.5 to 4.2 mass%).

3.4. Spinel formation

3.4.1. In situ spinel formation

As shown in Fig. 6, temperature has a marked influence on the dissolution rate of a MgO particle in slag A. Fig. 9 shows the dissolution curves of MgO in slag B at two different temperatures. Likewise, we observe that increasing the temperature increases

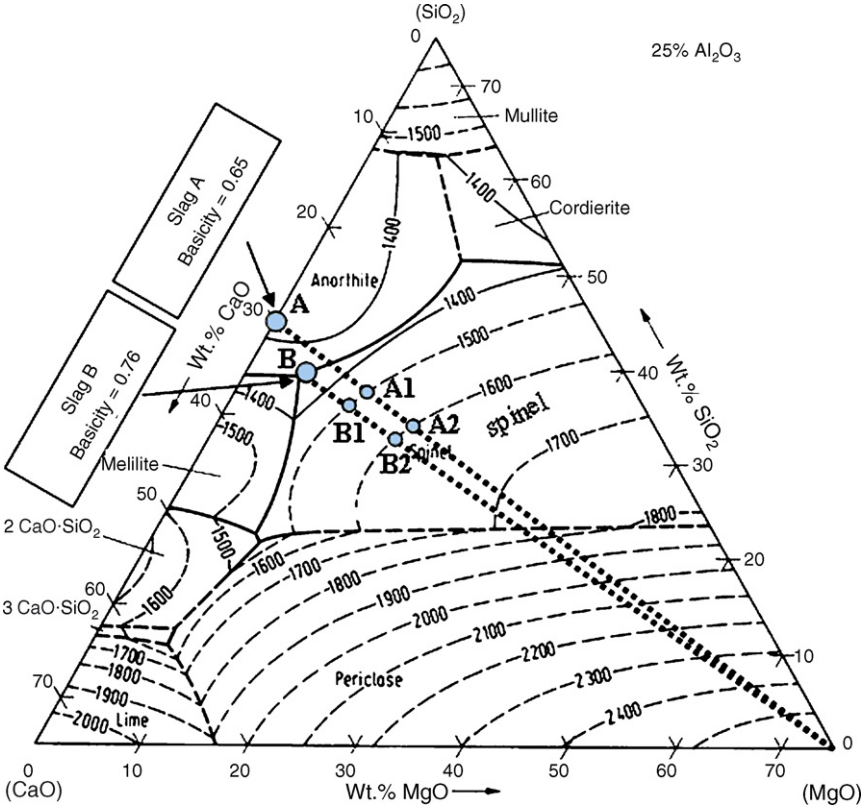

Fig. 8. Liquidus projection of the $CaO–Al_2O_3–SiO_2–MgO$ phase diagram.[23]

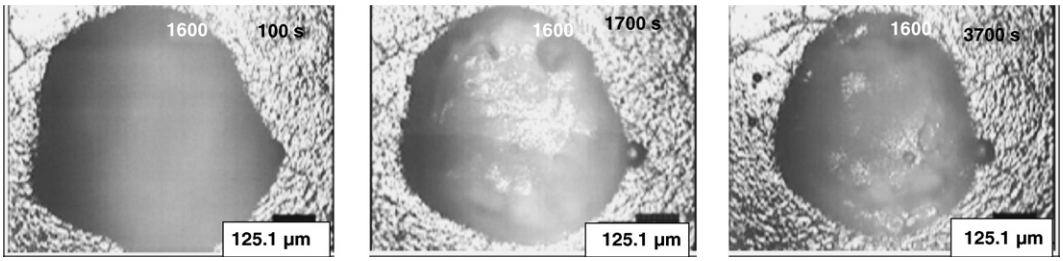

Fig. 10. Observation of a dissolving MgO particle in slag B at 1600 °C.

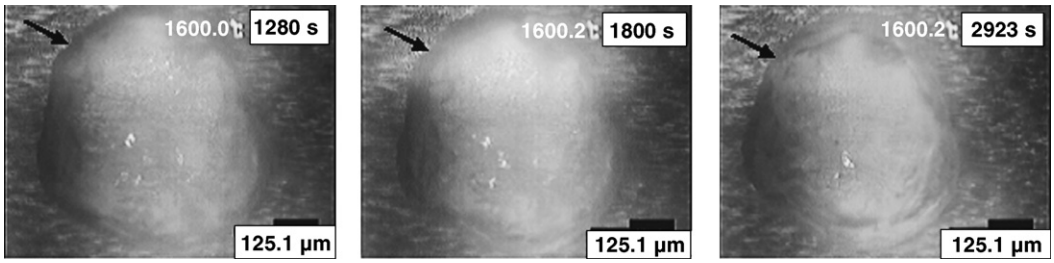

Fig. 11. Evolution of reaction layer around one MgO particle at 1600 °C in slag B.

the dissolution rate. However, it is necessary to point out that the real dissolution process as observed at 1600 °C in slag B is not simply described by the reduction of the equivalent radius. Indeed, during the dissolution process the focus plane of the laser was kept at the bottom of the crucible. It was observed that the MgO particle's transparency was altered with time. Fig. 10 shows that – although the diameter of the MgO particle did not change much during the dissolution process – the transparency of the particle first increased and later decreased. We suggest that the increase in transparency is related to a selective dissolution from the top and the bottom of the particle, which changes the spherical shape to a lenticular one with the same radius. We also suggest that the formation of a reaction layer thereafter decreases the transparency again. Shifting the focus plane to the upper surface of the particle, the evolution of the reaction layer can be seen (see Fig. 11). By the end of the dissolution experiment, large grains of the new product could be observed, as shown in Fig. 12.

3.4.2. *EPMA-WDS analysis of the particle/slag interface*

In order to investigate the reaction layer and to determine its chemical composition, the Pt crucible after the experiment at 1600 °C in slag B was sectioned. The interface between the particle and the slag was observed under the scanning electron microscope (SEM) and electron microprobe (EPMA). Fig. 13 shows the backscattered electron images of a cross section of the specimen taken with SEM. As shown in Fig. 13, the MgO particle did not dissolve completely within 90 min of experiment at 1600 °C in slag B. New products were formed during the dissolution process. EPMA-WDS analysis has shown that there are two new crystalline phases surrounding the partially dissolved MgO particle, namely, magnesia–alumina spinel phases and a CMS phase (monticellite). Two spinel layers were observed: outer (Fig. 13b) and inner spinel (Fig. 13c). Quantitative analysis of the inner spinel layer with EPMA-WDS yields a normalised composition of 30 wt.% MgO and 70 wt.% Al_2O_3. However, neither of these two spinel layers are continuous on this cross section of the specimen. The inner spinel layer was attached to the MgO particle at only a few points, which are believed to be the points of nucleation of spinel, and slag was trapped between the MgO particle and spinel (Fig. 13d). It is believed that this microstructure developed by sideways growth of spinel nuclei in the slag adjacent to the MgO particle. Sideways growth of spinel on sapphire in contact with silicate melts was also reported by Sandhage and Yurek[1] The outer spinel layer was found in the melt away from the MgO particle, as seen in Fig. 13b. Quantita-

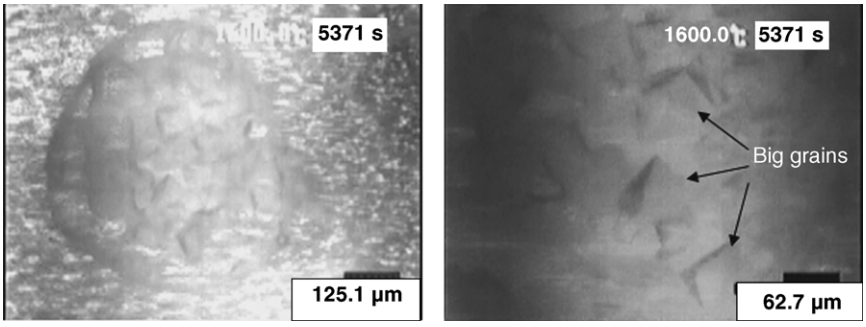

Fig. 12. MgO particle after dissolving in slag B at 1600 °C for 90 min.

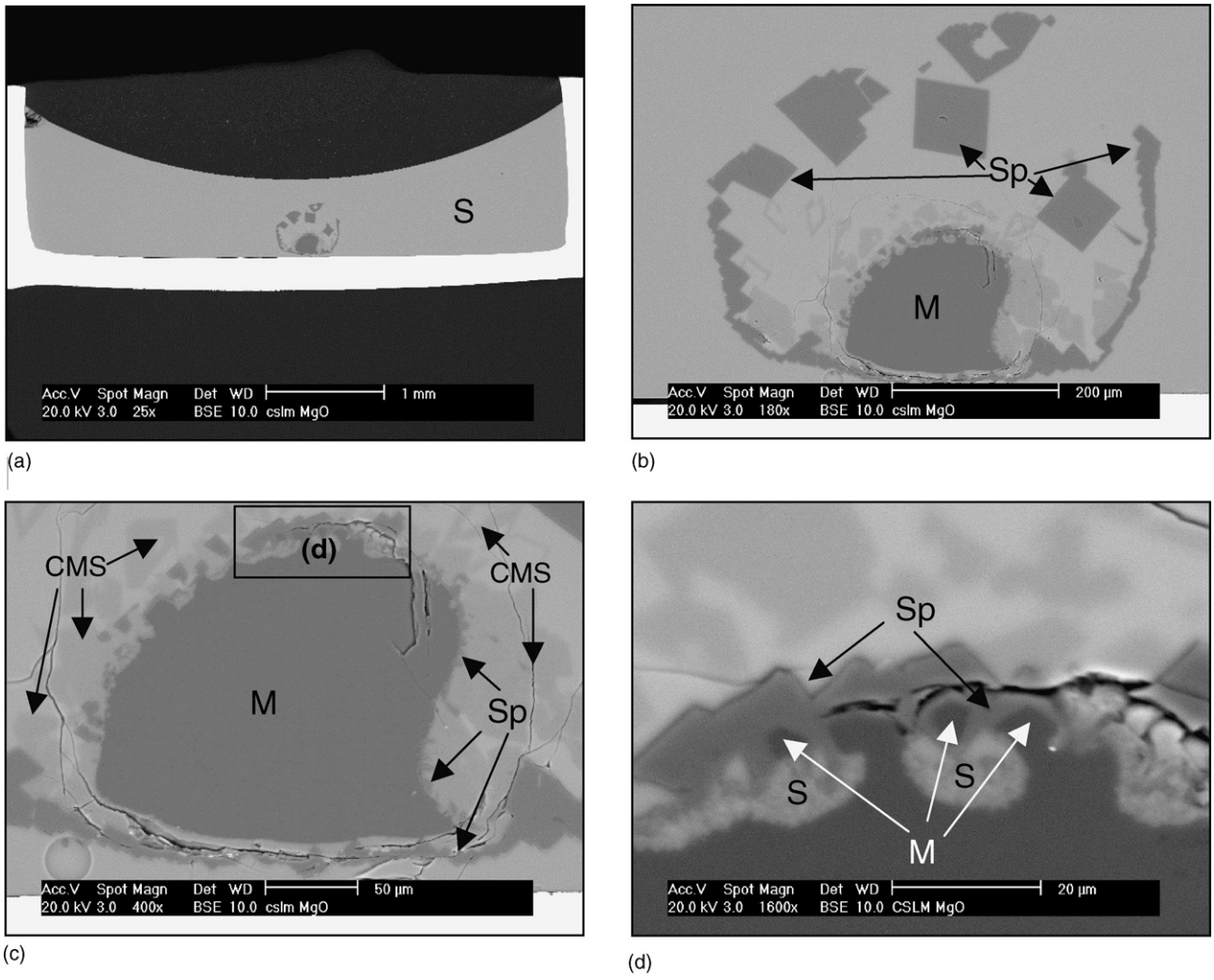

Fig. 13. Backscattered electron image of a cross section through a MgO particle that has been exposed to slag B at 1600 °C for 90 min (M = magnesia, Sp = magnesia–alumina spinel, S = slag, $C_xM_yS_z = xCaO{\cdot}yMgO{\cdot}zSiO_2$). (a) Overview of the specimen cross-section; (b) overview of the particle cross-section; (c) partially dissolved MgO at high magnification; (d) enlargement of small area in (c).

tive analysis of this spinel layer yields a normalised composition of 27 wt.% MgO and 73 wt.% Al_2O_3. It is believed that this spinel layer was formed due to the counter fluxes of dissolved MgO away from the MgO particle and Al_2O_3 from the bulk of the slag toward the MgO particle.[1] The CMS phases between two spinel layers were believed to be formed during cooling from the experimental temperature of 1600 °C.

3.4.3. Discussion on in situ spinel formation

Based on the *in situ* observation and characterisation with SEM and EPMA-WDS, the formation of *in situ* spinel is discussed now both from a thermodynamic and kinetic point of view.

3.4.3.1. Thermodynamics.

(a) Global equilibrium

Using the computational thermodynamics package Factsage© and the programming library ChemApp© it is possible to calculate stability diagrams in the investigated CMAS system. Fig. 14 shows these diagrams for 1500 and 1600 °C, and for basicities of 0.65 and 0.76, the basicities of slags A and B, respectively. As can be seen on the diagrams, the initial slag composition of both slags is in the fully liquid region at both temperatures, with or without MgO addition. Since the addition of the MgO from the particle only comprises a minor increase in the MgO content of the total system, the particle will be completely dissolved in the slag, from a thermodynamical point of ‘ view.

(b) Spinel formation

Although the final state of the system is complete dissolution of the particle in the slag, the global stability diagrams do not contain information on the path followed toward this global equilibrium. We show that for certain compositions of the slag in contact with the MgO particle, it is possible to lower the Gibbs free energy locally by forming spinel. The formation of a spinel layer on an MgO particle in a CASM

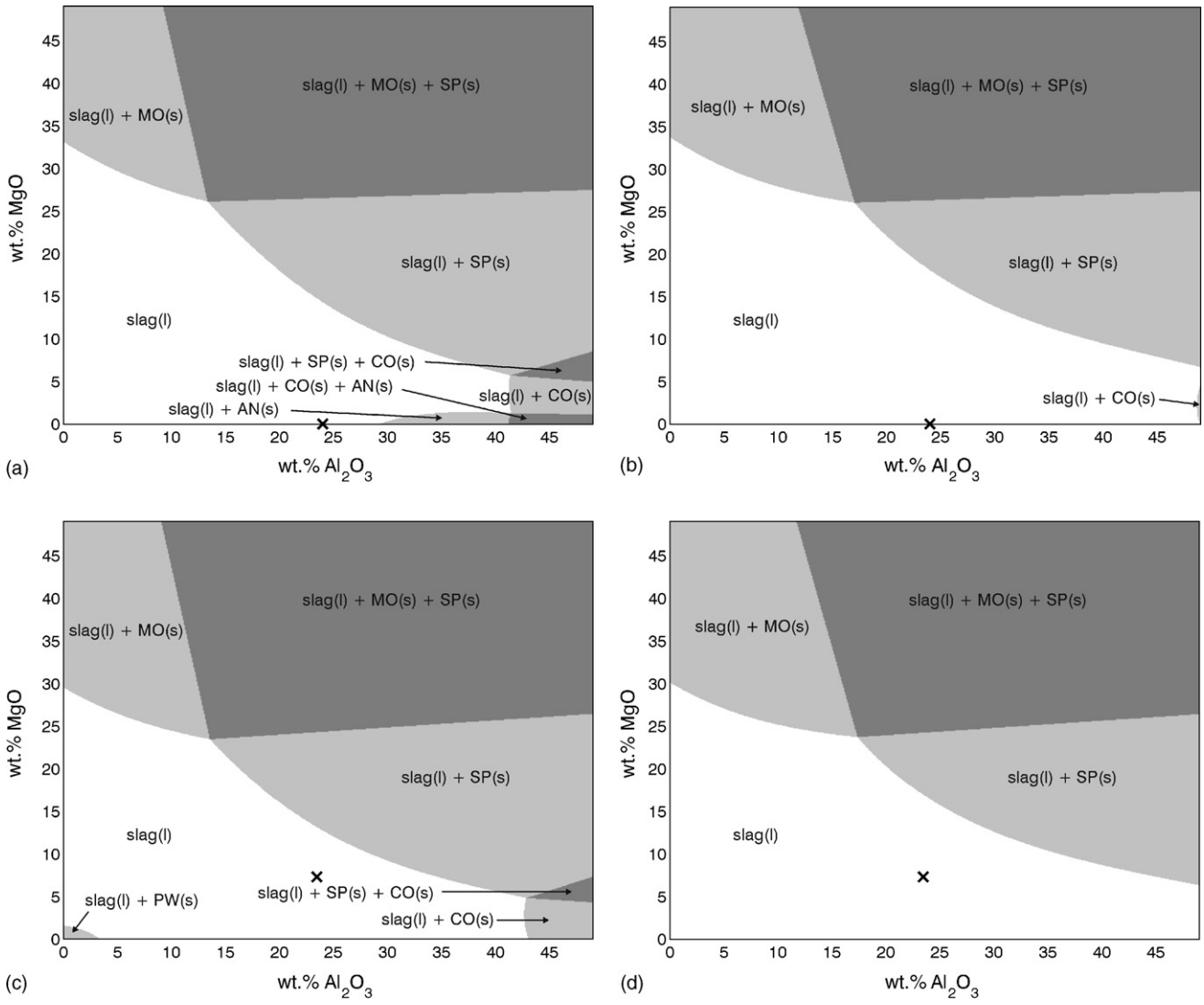

Fig. 14. Stability diagrams in the CMAS system (MO(s) = MgO-based solid solution, SP(s) = spinel, CO(s) = corundum (Al_2O_3), AN(s) = anorthite ($CaAl_2Si_2O_8$), PW(s) = pseudo-wollastonite ($CaSiO_3$); in (a) and (b) the cross indicates the initial composition of slag A, in (c) and (d) that of slag B): (a) 1500 °C, basicity = 0.65; (b) 1600 °C, basicity = 0.65; (c) 1500 °C, basicity = 0.76; (d) 1600 °C, basicity = 0.76.

melt can be represented by the reaction:

$$[MgO] + \{\underline{Al_2O_3}\}_{slag} = [MgAl_2O_4] \quad (3)$$

Using the above mentioned packages FactSage© and ChemApp©, we calculated the following equilibria:

$$[MgO] + \{\underline{Al_2O_3}\}_{slag} + \text{excess of slag} \Rightarrow \text{equilibrium} \quad (4)$$

and

$$[MgAl_2O_4] + \text{excess of slag} \Rightarrow \text{equilibrium} \quad (5)$$

For every reaction we calculate the change in Gibbs free energy. By subtracting these reactions, the spinel formation reaction is obtained. By subtracting in the same way the changes in Gibbs free energies of the reactions, the Gibbs free energy of the spinel formation reaction can be obtained. This is done for a range of slag compositions and is represented graphically in Fig. 15. As can be seen by comparing the different parts of Fig. 15, a lower temperature tends to stabilise spinel, a lower basicity extends the spinel stability region to higher MgO content, but tends to raise the required Al_2O_3 level. From these diagrams it can be concluded that for both slags, a thermodynamic driving force for spinel formation exists at both 1500 and 1600 °C. Whether or not spinel will form, depends on kinetic factors.

3.4.3.2. Kinetics. Once the thermodynamic conditions for spinel formation on MgO (Eq. (5)) in a CASM melt are satisfied, spinel can nucleate and grow on MgO. The amount and morphology of the spinel that actually forms are related to kinetic factors. According to Sandhage and Yurek[1] a number of steps are involved in the nucleation of spinel on MgO that is immersed into a CASM slag: (1) Aluminium- and oxygen-bearing ions diffuse to and adsorb on the MgO particle. (2) Breakup of any complex ions that may be involved occurs at the surface. (3) Surface diffusion of adsorbed ions occurs. (4) Critical concentration of aluminium, magnesium, and oxygen ions collect at nucleation

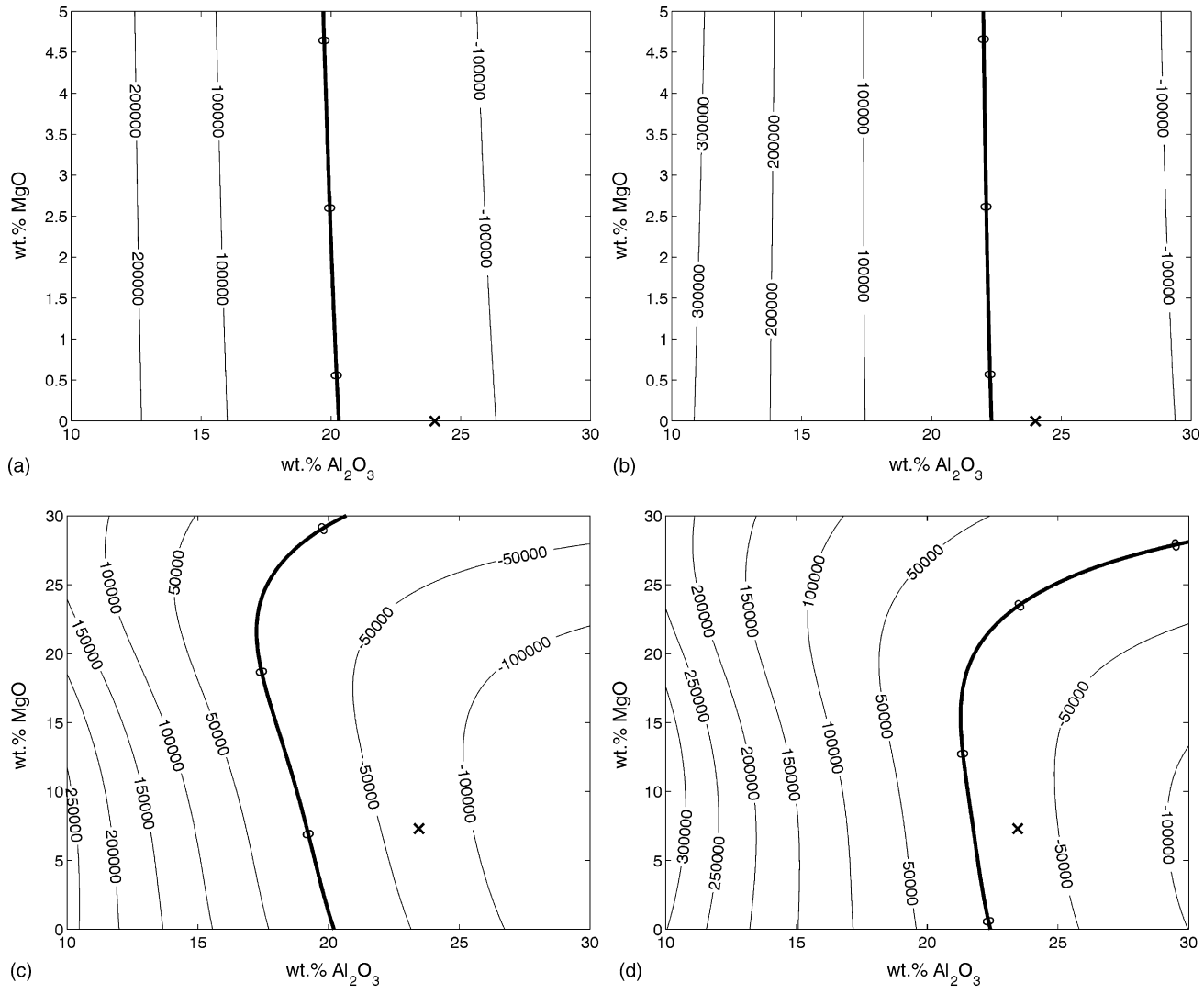

Fig. 15. Reaction Gibbs free energy for the spinel formation reaction (in (a) and (b) the marker indicates the initial composition of slag A, in (c) and (d) that of slag B): (a) 1500 °C, basicity = 0.65; (b) 1600 °C, basicity = 0.65; (c) 1500 °C, basicity = 0.76; (d) 1600 °C, basicity = 0.76.

sites to form nuclei of MgO-saturated spinel. The exact nature of the aluminium- and oxygen-bearing ions that are present in the slag is not known. It is unlikely, however, that transport of Mg from the MgO particle into the slag, or of Al from the slag to the MgO particle, involves molecules of MgO or Al_2O_3. Tracer diffusion experiments in $CaO–Al_2O_3–SiO_2$ melts at temperatures above 1400 °C have shown that oxygen ions diffuse one order of magnitude faster than Al or Ca ions.[24–26] Therefore, the fluxes of Mg and Al can be described in terms of effective oxide fluxes by assuming that when cation diffusion occurs, the oxygen anions distribute themselves rapidly to maintain electroneutrality. Thus, the dissolution of MgO into the slag will be discussed in terms of an effective flux of MgO into the slag, and the transport of Al in the slag toward the MgO particle is discussed in terms of an effective flux of Al_2O_3.

The extent to which initially formed nuclei can grow, depends on the relative fluxes of MgO away from the MgO particle and of Al_2O_3 toward the MgO. Upon nucleation and growth of spinel on the surface of an MgO particle, the slag near the spinel becomes depleted in Al_2O_3, and additional Al_2O_3 must diffuse from the surrounding slag to the spinel particles to enable their further growth. At the same time, however, because the bulk slag is unsaturated with respect to MgO, the MgO particle dissolves into the slag. This increases the MgO concentration in the slag near the MgO particle, thereby decreasing the local Al_2O_3 content. The local reduction in the Al_2O_3 content of the slag, which is caused by both spinel nucleation and dissolution of the MgO particle, could inhibit growth of spinel nuclei. It could also prevent additional nucleation of spinel on the MgO particle by decreasing the supersaturation at the MgO/slag interface. Dissolution of MgO into unsaturated slag occurs from the initial stage onward, although it is inhibited in locations where particles of spinel have nucleated. The countercurrent flux of Al_2O_3 in the slag toward the MgO particle could yield homogeneous nucleation of spinel particles in the slag adjacent to the MgO particle. However, sideways growth of existing spinel might require less supersaturation in the slag and, thus, could be energetically more favorable. Thus, the spinel layer has serrated edges on the MgO

particle side and slag was trapped between the MgO particle and the spinel layer.

Once a continuous spinel layer covers the MgO particle (e.g. MgO particles indicated by arrows in Fig. 13d), the MgO particle continues to dissolve into the slag through an *indirect dissolution* process. The spinel layer increases in thickness by formation of spinel at the MgO/spinel interface, and it decreases in thickness by dissociation at the spinel/slag interface. A steady-state thickness of the spinel is achieved when the rates of growth and dissociation become equal.

Growth of spinel on MgO that is put into contact with a source of Al_2O_3 occurs by countercurrent, solid-state transport of equivalent amounts of Mg^{2+} and Al^{3+} through the spinel.[27,28] Transport of oxygen anions is negligible. Al^{3+} ions that arrive at the MgO/spinel interface react with MgO to form spinel and release Mg^{2+} cations that diffuse through the spinel to the spinel/slag interface (Eq. (6)). At the latter interface, the spinel dissociates to release Al^{3+} cations and the MgO dissolves in the slag (Eq. (7)). The Al^{3+} cations released at the spinel/slag interface diffuse to the MgO/spinel interface where they react with MgO to continue the cycle. At steady state, no additional Al_2O_3 is removed from the slag to form spinel. The net effect of reactions in Eqs. (6) and (7) is the transfer of MgO from the MgO particle to the slag (Eq. (8)). Because this dissolution process involves transport through an intermediate phase, it is called "indirect dissolution." A schematic model for the steady state, indirect dissolution of an MgO particle into a CASM melt is shown in Fig. 16:

$$4MgO + 2Al^{3+} = MgAl_2O_4 + 3Mg^{2+} \quad (6)$$

$$MgAl_2O_4 + 3Mg^{2+} = 2Al^{3+} + 4\{\underline{MgO}\}_{slag} \quad (7)$$

$$\text{net reaction}: \quad 4MgO = 4\{\underline{MgO}\}_{slag} \quad (8)$$

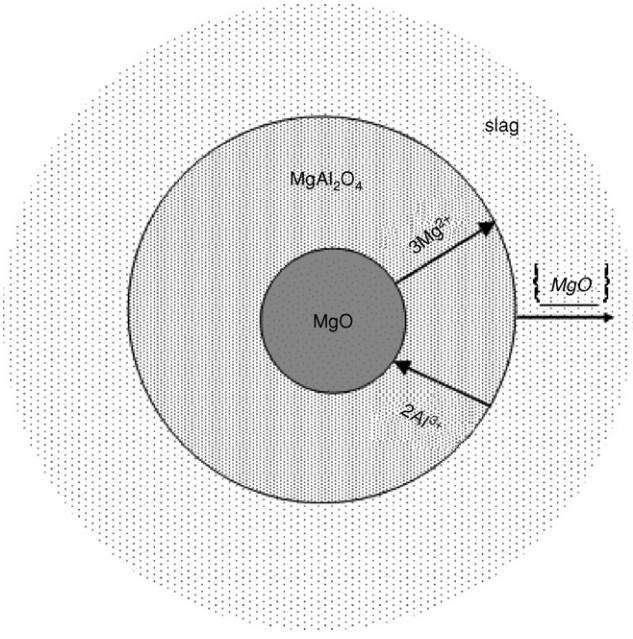

Fig. 16. Schematic model for the steady state, indirect dissolution for an MgO particle into a CASM melt.

4. Conclusions

The dissolution of MgO particles in high silica calcia–alumina–silica-based slags, has been studied *in situ* at 1500 and 1600 °C by using a CSLM with an infrared image furnace. The CSLM technique is shown to be effective for direct observation of refractory corrosion by metallurgical slags. Any plane between the bottom of the crucible and the top surface of the slag can be observed on the condition that the slag is transparent to laser light:

(1) The main features observed during the dissolution process are: (a) rotation of non-spherical particles and (b) rounding of angular particles.
(2) Temperature and MgO content in the original slag have outspoken effects on the dissolution process. Increasing the temperature enhances the dissolution rate. Addition of MgO to the slag delays the dissolution time of the MgO particle significantly.
(3) MgO dissolution is primarily controlled by a boundary layer diffusion mechanism, although the actual dissolution curves do not perfectly fit the theoretical curve, which can be explained by inaccuracies associated with the present procedure.
(4) In the case of the dissolution in slag B at 1600 °C, a dark reaction layer could be observed. According to EPMA-WDS analysis, it was shown to be $MgAl_2O_4$ spinel. Once a continuous spinel layer covered the MgO particle, the MgO particle continued to dissolve into the slag through an *indirect dissolution* process. These direct observations were supported by kinetic considerations and thermodynamic calculations. The latter showed that it is important to distinguish between the global equilibrium and the local equilibrium in the vicinity of the magnesia particle. Global equilibrium data do not contain information on the path followed toward this global equilibrium. This explains why, even though globally no spinel is expected to form under the present conditions, for certain compositions of the slag in contact with the MgO particle, it was possible to lower the Gibbs free energy locally by forming spinel.
(5) Finally, these findings are both relevant for refractory applications and clean steel production. In the former one targets (slow) indirect dissolution to enhance the refractory lifetime, while in the latter it is desirable that no intermediate spinel layer is formed to allow for rapid dissolution kinetics into the slag and to avoid re-entrainment of MgO inclusions into the steel.

Acknowledgements

Eddy Boydens and Pieter L'hoëst are acknowledged for the EMPA-WDS analysis and useful discussions in this work.

References

1. Sandhage, K. H. and Yurek, G. J., Indirect dissolution of sapphire into silicate melts. *J. Am. Ceram. Soc.*, 1988, **71**(6), 478–489.

2. Matsushima, M., Yadoomaru, S., Mori, K. and Kawai, Y., A fundamental study on the dissolution rate of solid lime into liquid slag. *Trans. Iron Steel Inst. Jpn.*, 1977, **17**, 442–449.
3. Kimura, H., Yanagase, T., Noguchi, F. and Ueda, Y., Studies on the mechanism of CaO dissolution into slag melts. *Nippon Kinzoku Gakkaishi*, 1974, **38**, 226–232.
4. Sandhage, K. and Yurek, G., Indirect dissolution of sapphire into calcia–magnesia–alumina–silica melts: electron microprobe analysis of the dissolution process. *J. Am. Ceram. Soc.*, 1990, **73**(12), 3643–3649.
5. Bygden, J., Debroy, T. and Seetharaman, S., Dissolution of MgO in stagnant CaO–FeO–SiO_2 slags. *Ironmak. Steelmak.*, 1994, **21**, 318–323.
6. Allen, N., Sun, S. and Jahanshahi, S., Stability of MgO refractory in contact with iron-rich slags. In *Proceedings of the Second Melt Chemistry Symposium*, 1995, pp. 55–59.
7. Zhang, P. and Seetharaman, S., Dissolution of MgO in CaO–'FeO'–CaF_2–SiO_2 slags under static conditions. *J. Am. Ceram. Soc.*, 1994, **77**, 970–976.
8. Zhang, S., Sarpoolaky, H., Marriott, N. J. and Lee, W. E., Penetration and corrosion of magnesia grain by silicate slags. *Br. Ceram. Trans.*, 2000, **99**(6), 248–255.
9. Valdez, M., Prapakorn, K., Sridhar, S. and Cramb, A. W., Dissolution of inclusions in steelmaking slags. In *Proceedings of the ISSTech 2003 Conference*, 2003, pp. 789–798.
10. Satyoko, Y. and Lee, W. E., Dissolution of dolomite and doloma in silicate slag. *Br. Ceram. Trans.*, 1999, **98**(6), 261–265.
11. Sandhage, K. and Yurek, G., Direct and indirect dissolution of sapphire in calcia–magnesia–alumina–silica melts. *J. Am. Ceram. Soc.*, 1990, **73**, 3633–3642.
12. Valdez, M., Prapakorn, K., Cramb, A. W. and Seetharaman, S., A study of the dissolution of Al_2O_3, MgO and $MgAl_2O_4$ particles in a CaO–Al_2O_3–SiO_2 slag. *Steel Res.*, 2001, **72**(8), 291–297.
13. Monaghan, B. J., Nightingale, S. A., Chen, L. and Brooks, G. A., The dissolution behavior of selected oxides in CaO–SiO_2–Al_2O_3 slags. In *Proceedings of the VII International Conference on Molten Slags and Salts*, 2004, pp. 585–594.
14. Yi, K. W., Tse, C., Park, J.-H., Valdez, M., Cramb, A. W. and Sridhar, S., Determination of dissolution time of Al_2O_3 and MgO inclusions in synthetic Al_2O_3–CaO–MgO slags. *Scand. J. Metall.*, 2003, **32**, 177–184.
15. Sridhar, S. and Cramb, A. W., Kinetics of Al_2O_3 dissolution in CaO–MgO–SiO_2–Al_2O_3 slags: in situ observations and analysis. *Metall. Mater. Trans. B*, 2000, **31**, 406–410.
16. Orrling, C., Fang, Y., Phinichka, N., Sridhar, S. and Cramb, A. W., Observing and measuring solidification phenomena at high temperatures. *JOM-e*, 1999, **51**(7), Available at http://www.tms.org/pubs/journals/JOM/9907/Orrling/Orirling-9907.html.
17. Orrling, C., Sridhar, S. and Cramb, A. W., *In situ* observation of the role of alumina particles on the crystallization behavior of slags. *ISIJ Int.*, 2000, **40**, 877–885.
18. Bonar, J. A., Kennedy, C. R. and Swaroop, R. B., Coal–ash slag attack and corrosion of refractories. *Am. Ceram. Soc. Bull.*, 1980, **59**(4), 473–478.
19. Kennedy, C. R., Compatibility of water-cooled chromia-containing refractories with a high iron oxide acidic coal–ash slag at 1575 °C. *J. Mater. Energy Syst.*, 1981, **3**, 39–47.
20. NIH Image, version 1.62, developed at U.S. National Institute of Health and available on the internet at http://rsb.info.nih.gov/nih-image/.
21. Lee, W. E. and Zhang, S., Melt corrosion of oxide and oxide-carbon refractories. *Int. Mater. Rev.*, 1999, **44**(3), 77–104.
22. Levenspiel, O., *Chemical reaction engineering* (*3rd ed.*). John Wiley & Sons, New York, 1999 [Chapter 25].
23. *Verein deutscher Eisenhüttenleute*, *Schlachenatlas* (*Slag atlas*), 2nd ed., 1995, p. 158, ISBN 3-514-00457-9.
24. Towers, H., Paris, M. and Chipman, J., Diffusion of calcium ion in liquid slag. *Trans. Metall. Soc. AIME*, 1953, **197**, 1455–1458.
25. Henderson, J., Yang, L. and Derge, G., Self-diffusion of aluminum in CaO–SiO_2–Al_2O_3 melts. *Trans. Metall. Soc. AIME*, 1961, **221**, 56–60.
26. Koros, P. J. and King, T. B., The self-diffusion of oxygen in a lime–silica–alumina slag. *Trans Metall. Soc. AIME*, 1962, **224**, 229–306.
27. Carter, R. E., Mechanism of solid-state reaction between magnesium oxide and aluminum oxide and between magnesium oxide and ferric oxide. *J. Am. Ceram. Soc*, 1961, **44**(3), 116–120.
28. Rossi, R. C. and Fulrath, R. M., Epitaxial growth of spinel by reaction in the solid state. *J. Am. Ceram. Soc.*, 1963, **46**(3), 145–149.